Reduction of air space behind piezoelectric absorbing panel using negative stiffness

Keisuke YAMADA[1]; Kenta YAMAGATA[2]; Hideo UTSUNO[3]

[1] Kansai University, Japan

[2] Kyoto University, Japan

[3] Kansai University, Japan

ABSTRACT

This paper proposes a method of reduction of the air space behind the piezoelectric sound absorbing panel using the piezoelectric elements, negative capacitor, and resistor. Because the air space behind the panel works as an air spring, the natural frequency of the panel is increased by the air spring under the condition that the air space is small. Therefore, the purpose of this research is to decrease the increased natural frequency of the piezoelectric sound absorbing panel due to the air space behind the panel. The negative capacitor and resistor are coupled to the piezoelectric elements bonded on the panel. The piezoelectric elements and circuit give negative stiffness and positive damping to the panel. The governing equations were theoretically derived, and optimum values of the negative capacitance and resistance were respectively formulated. The effectiveness of the proposed method and the theoretical analysis were verified through simulations and experiments.

Keywords: Sound absorption, Piezoelectric element, Low frequency noise
I-INCE Classification of Subjects Number(s): 35.7, 38.5.1

1. INTRODUCTION

To provide a silent space, noise sources should be removed. In case where the noise sources cannot be removed, vibration of the noise sources should be suppressed. When noise reduction is still insufficient despite these measures, the noise itself must be suppressed. In general, porous sound absorbing materials are used for noise reduction. The porous sound absorbing materials dissipate sound energy through the viscosity on the surface of the materials. Therefore, sound absorption effect is low in the low frequency region if the materials are placed on the walls.

Sound absorption using vibration of plates is well known. This method uses the resonance of the plates. Because the mechanical impedance of the plates is small around the resonance frequency, the sound energy flows into the plate. The vibration energy of the plates is dissipated through the damping of the plates. This method has an advantage that the low-frequency noise can be absorbed; however, the damping ratio of the plates is usually insufficient for optimum condition. To solve this problem, piezoelectric sound absorbing panel was proposed (1). Piezoelectric elements are bonded on the plate and an LR circuit is coupled to the piezoelectric elements in this method. The electrical resonance between the capacitance of the piezoelectric elements and LR circuit gives damping effect to the plate (2). This method is effective; however, reduction of the air space behind the plate induces increase of resonance frequency because the air space works as an air spring. The reduction of the air space is critical to downsizing of the device, we presents a new piezoelectric sound absorbing panel that uses negative stiffness in this paper. Negative capacitor coupled to the piezoelectric elements equivalently works as negative stiffness (3). Therefore, the new piezoelectric sound absorbing panel uses the negative capacitor and resistor to tune the resonance frequency and

[1] yamadak@kansai-u.ac.jp
[2] yamagata.kenta.75e@st.kyoto-u.ac.jp
[3] utsuno@kansai-u.ac.jp

damping ratio of the plate. In this research, we derive the normal incidence sound absorption coefficient of the plate. The optimum values of the negative capacitance and resistance are derived. Here, the purpose of the optimization of the circuit is maximization of the normal incidence sound absorption coefficient at the targeted frequency. The effectiveness of the proposed method and theoretical analysis is verified through simulations and experiments.

2. THEORETICAL ANALYSIS

2.1 Analytical Model

The analytical model of the proposed method is shown in Figure 1. The piezoelectric sound absorbing panel using the negative capacitor and resistor is placed at the right end of the one-dimensional acoustic tube. The piston at the left end is the sound source. Only the fundamental vibration mode of the plate is used in this study. The sealed air on the right-hand side of the plate works as an air spring. The acoustic fields on the left-hand and right-hand sides of the plate are referred to as acoustic field 1 and 2, respectively. The lengths of the acoustic fields 1 and 2 are l_1 and l_2, respectively. In this theoretical analysis, the dielectric loss tangents of the piezoelectric element and negative capacitor are considered because the internal loss in them cannot be neglected. The complex capacitances of the piezoelectric element and negative capacitor are respectively given as

$$C_p^* = C_p \big/ \left(1 + \mathrm{j}\tan\delta_C\right) \tag{1}$$

$$C_N^* = C_N \big/ \left(1 + \mathrm{j}\tan\delta_N\right) \tag{2}$$

where C_p is the capacitance of the piezoelectric element, C_N is the capacitance of the negative capacitor, $\tan\delta_C$ is the dielectric loss tangent of the piezoelectric element, $\tan\delta_N$ is the dielectric loss tangent of the negative capacitor, and j is the imaginary unit. The resistance of the resistor is R as shown in Figure 1.

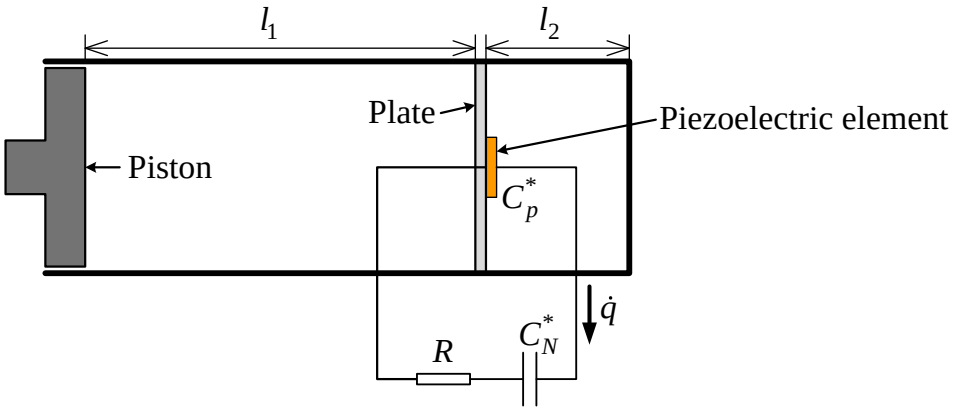

Figure 1 – One dimensional acoustic tube with a piezoelectric sound absorbing panel.

2.2 Specific Acoustic Impedance Ratio

The sound pressures on the left-hand and right-hand surfaces of the plate are referred to as p_1 and p_2, respectively. Because the effect of the sound absorption is provided around the natural frequency of the fundamental vibration mode of the plate, the influence of the other vibration modes of the plate is neglected in this theoretical analysis. The equation of motion of the fundamental vibration mode of the piezoelectric sound absorbing panel is given as

$$M\ddot{\xi} + D\dot{\xi} + K\xi + \Theta\left(\Theta\xi \big/ C_p^* - q \big/ C_p^*\right) = \int_A \Psi \mathrm{d}A\left(p_1 - p_2\right) \tag{3}$$

where M is the modal mass, D is the modal damping coefficient, K is the modal stiffness, Θ is the modal electromechanical coupling coefficient, ξ is the modal displacement, q is the charge stored in the piezoelectric element, Ψ is the eigenfunction of the fundamental vibration mode, and A is the area of the plate. The circuit equation is expressed as

$$R\dot{q} + q/C_N^* = \Theta\dot{\xi}/C_p^* - q/C_p^* \tag{4}$$

To derive the specific acoustic impedance of the piezoelectric sound absorbing panel on the left-hand surface, the sound pressure p_1 and particle velocity are required. Because the vibration shape of the plate is determined by the eigenfunction Ψ, the particle velocity is not uniform. Therefore, the particle velocity is given by the average in this research. The average of the displacement of the plate is expressed as

$$w_1 = \int_A \Psi \mathrm{d}A\xi / A \tag{5}$$

Using Eq. (5), the equation of motion and circuit equation are respectively given as

$$M_b\ddot{w}_1 + D_b\dot{w}_1 + K_b w_1 + \Theta_b\left(\Theta_b w_1/C_p^* - q/C_p^*\right) = A\left(p_1 - p_2\right) \tag{6}$$

$$R\dot{q} + q/C_N^* = \Theta_b\dot{\xi}/C_p^* - q/C_p^* \tag{7}$$

where

$$M_b = M\left(A/\int_A \Psi \mathrm{d}A\right)^2,\quad D_b = D\left(A/\int_A \Psi \mathrm{d}A\right)^2,\quad K_b = K\left(A/\int_A \Psi \mathrm{d}A\right)^2,\quad \Theta_b = \Theta\left(A/\int_A \Psi \mathrm{d}A\right) \tag{8–11}$$

In addition, the electrical system can be transformed into the equivalent mechanical model (2). Using the equivalent mechanical model, the equation of motion and circuit equation can be expressed as

$$M_b\ddot{w}_1 + D_b\dot{w}_1 + K_b w_1 + K_C^*\left(w_1 - w_2\right) = A\left(p_1 - p_2\right) \tag{12}$$

$$D_R\dot{w}_2 + K_N^* w_2 + K_C^*\left(w_2 - w_1\right) = 0 \tag{13}$$

where

$$D_R = R\Theta_b^2,\quad K_C^* = K_C\left(1 + \mathrm{j}\tan\delta_C\right),\quad K_N^* = K_N\left(1 + \mathrm{j}\tan\delta_N\right), \tag{14–16}$$

$$K_C = \Theta_b^2/C_p,\quad K_N = \Theta_b^2/C_N,\quad w_2 = q/\Theta_b \tag{17–19}$$

The sound pressure p_2 is determined by the specific acoustic impedance of the air space and particle velocity on the right-hand surface of the plate. The specific acoustic impedance of the air space is given as

$$z_2 = -\mathrm{j}\rho_a c_a/\tan kl_2 \tag{20}$$

where ρ_a is the density of the air, c_a is the speed of the sound in the air, and k is the wave number. Because l_2 is sufficiently smaller than the wavelength of sound, the air space works as an air spring. From Eq. (20), the spring constant of the air spring is expressed as

$$K_a = \rho_a c_a^2 A/l_2 \tag{21}$$

Using Eq. (21), the equation of motion is given as

$$M_b\ddot{w}_1 + D_b\dot{w}_1 + \left(K_b + K_a\right)w_1 + K_C^*\left(w_1 - w_2\right) = Ap_1 \tag{22}$$

Using Eqs. (13) and (22), the analytical model can be transformed into the concentrated mass model shown in Figure 2. Here

$$K_T = K_b + K_a \tag{23}$$

Because the spring constant of the air spring is inversely proportional to the length of the air space, the natural frequency of the piezoelectric sound absorbing panel increases with the decrease of l_2. From Eqs. (13) and (22), the specific acoustic impedance of the piezoelectric sound absorbing

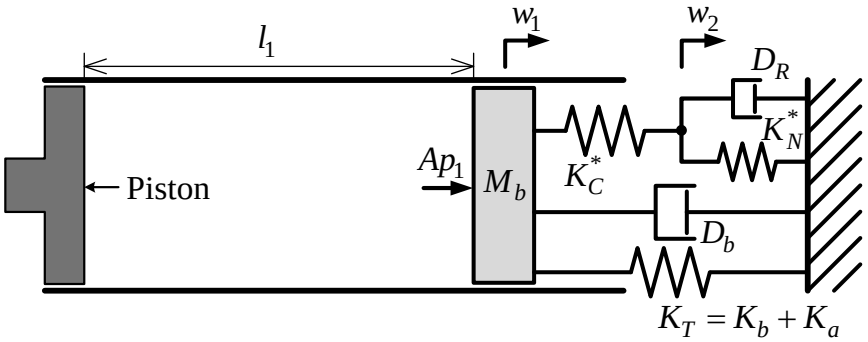

Figure 2 – Analytical model using concentrated mass model.

panel on the left-hand surface of the plate is expressed as

$$z=\frac{K_T}{\mathrm{j}\omega A}\left\{-g^2+2\mathrm{j}\gamma g+1+\beta_T\left(1+\mathrm{j}\tan\delta_C\right)\frac{\eta+\mathrm{j}\eta\left(-\zeta_R g+\tan\delta_N\right)}{1+\eta+\mathrm{j}\left(\tan\delta_C+\eta\tan\delta_N-\eta\zeta_R g\right)}\right\} \tag{24}$$

where

$$g=\omega/\Omega,\quad \gamma=D_b\Big/\left(2\sqrt{M_bK_T}\right),\quad \beta_T=K_C/K_T, \tag{25–27}$$

$$\eta=K_N/K_C,\quad \zeta_R=-\Omega D_R/K_N,\quad \Omega=\sqrt{K_T/M_b} \tag{28–30}$$

The specific acoustic impedance ratio of the piezoelectric sound absorbing panel is given as

$$\bar{z}=\frac{\lambda}{\mathrm{j}g}\left\{-g^2+2\mathrm{j}\gamma g+1+\beta_T\left(1+\mathrm{j}\tan\delta_C\right)\frac{\eta+\mathrm{j}\eta\left(-\zeta_R g+\tan\delta_N\right)}{1+\eta+\mathrm{j}\left(\tan\delta_C+\eta\tan\delta_N-\eta\zeta_R g\right)}\right\} \tag{31}$$

where λ is the acoustic characteristic impedance ratio defined as follows:

$$\lambda=\sqrt{M_bK_T}\Big/\left(\rho_a c_a A\right) \tag{32}$$

2.3 Normal Incidence Sound Absorption Coefficient and Optimum Tuning of Circuit

The normal incidence sound absorption coefficient of the piezoelectric sound absorbing panel is expressed as

$$\alpha=1-\left|\left(z-\rho_a c_a\right)/\left(z+\rho_a c_a\right)\right|^2=1-\left|(\bar{z}-1)/(\bar{z}+1)\right|^2 \tag{33}$$

In this research, the object of the optimum tuning of the circuit is to maximize the value of the normal incidence sound absorption coefficient at a targeted frequency. From Eq. (33), the real part of the specific acoustic impedance ratio should be 1, and imaginary part should be 0. In this research, the values of the negative stiffness ratio η and resistance ratio ζ_R are tunable. The negative stiffness ratio and resistance ratio that achieve $\bar{z}=1$ at a targeted excitation frequency ratio g_a should be derived using Eq. (31); however, the solutions cannot be obtained using Eq. (31). Therefore, we use the equivalent dielectric loss tangent instead of the resistance ratio ζ_R. The relation between the resistance ratio ζ_R and equivalent dielectric loss tangent $\tan\delta_R$ is given as

$$\zeta_R=-\tan\delta_R/g \tag{34}$$

Because the dielectric loss tangent $\tan\delta_R$ is constant, Eq. (34) is exact at only one excitation frequency ratio. However, there is no problem in this derivation of the optimum values of the circuit because the proposed method can satisfy $\bar{z}=1$ at only the targeted excitation frequency ratio. Therefore, Eq. (34) should be satisfied at $g=g_a$. Using Eq. (34), the specific acoustic impedance ratio is simplified as

$$\bar{z}=\frac{\lambda}{\mathrm{j}g}\left\{-g^2+2\mathrm{j}\gamma g+1+\eta\beta_T\frac{1+\tan^2\delta_C+\eta\left(1+\tan^2\delta_{RN}\right)+\mathrm{j}\left[\tan\delta_{RN}\left(1+\tan^2\delta_C\right)+\eta\tan\delta_C\left(1+\tan^2\delta_{RN}\right)\right]}{\left(1+\eta\right)^2+\left(\tan\delta_C+\eta\tan\delta_{RN}\right)^2}\right\} \tag{35}$$

$$\tan\delta_{RN}=\tan\delta_R+\tan\delta_N \tag{36}$$

The optimum negative stiffness ratio η_{opt} and optimum dielectric loss tangent $\tan\delta_{RNopt}$ can be derived under the condition that $\bar{z}=1$ at $g=g_a$.

$$\eta_{opt}=-\frac{g_a^4+g_a^2\left[\left(\lambda^{-1}-2\gamma\right)^2-2-\beta_T\left(1+\tan^2\delta_C\right)\right]+1+\beta_T\left(1+\tan^2\delta_C\right)}{g_a^4+g_a^2\left[\left(\lambda^{-1}-2\gamma\right)^2-2\left(1+\beta_T\right)\right]-2g_a\beta_T\left(\lambda^{-1}-2\gamma\right)\tan\delta_C+\left(1+\beta_T\right)^2+\beta_T^2\tan^2\delta_C} \tag{37}$$

$$\tan\delta_{RNopt}=\frac{g_a^4\tan\delta_C+g_a^2\left[\left(\lambda^{-1}-2\gamma\right)^2-2\right]\tan\delta_C-g_a\beta_T\left(\lambda^{-1}-2\gamma\right)\left(1+\tan^2\delta_C\right)+\tan\delta_C}{g_a^4+g_a^2\left[\left(\lambda^{-1}-2\gamma\right)^2-2-\beta_T\left(1+\tan^2\delta_C\right)\right]+1+\beta_T\left(1+\tan^2\delta_C\right)} \tag{38}$$

From Eqs. (36) and (38), the optimum dielectric loss tangent $\tan\delta_{Ropt}$ is given as

$$\tan\delta_{Ropt}=\tan\delta_{RNopt}-\tan\delta_N \tag{39}$$

From Eqs. (34) and (39), the optimum resistance ratio ζ_{Ropt} is derived as

$$\zeta_{Ropt}=-\frac{\tan\delta_{Ropt}}{g_a} \tag{40}$$

Using η_{opt} and ζ_{Ropt}, the optimum values of the negative capacitance and resistance can be obtained. The optimum value of the resistance can be negative depending on the conditions.

2.4 Effect of Equivalent Stiffness Ratio and Acoustic Characteristic Impedance Ratio

The exact specific acoustic impedance ratio is given by Eq. (31). The specific acoustic impedance ratio given by Eq. (35) is exact only at $g = g_a$; however, Eq. (35) gives good approximation around $g = g_a$. Because the specific acoustic impedance is expressed by a simple formula using Eq. (35), the characteristics of the proposed method is theoretically analyzed using Eq. (35) in this section. Substitution of Eqs. (37) and (38) into Eq. (35) yields

$$\bar{z} = \lambda\left\{-g^2 + g_a^2 + \mathrm{j}\left[2\gamma g + g_a\left(\lambda^{-1} - 2\gamma\right)\right]\right\}\Big/\mathrm{j}g \tag{41}$$

From Eqs. (33) and (41), the normal incidence sound absorption coefficient is expressed as

$$\alpha = 4g\left[2\gamma\lambda\left(g - g_a\right) + g_a\right]\Big/\left\{\left[g + g_a + 2\gamma\lambda\left(g - g_a\right)\right]^2 + \lambda^2\left(g - g_a\right)^2\left(g + g_a\right)^2\right\} \tag{42}$$

Because the equivalent stiffness ratio β_T is not included in Eq. (42), the normal incidence sound absorption is independent of the equivalent stiffness ratio under the optimum condition. In addition, Eq. (42) indicates that the width of the frequency range that gives a high value of the sound absorption coefficient is inversely proportional to the value of the acoustic characteristic impedance ratio λ. In other words, the performance of the proposed method only depends on the value of the acoustic characteristic impedance of the plate. From this perspective, the equivalent mass M_b and equivalent stiffness K_T should be small, whereas the area of the plate A should be large.

3. SIMULATION

The effectiveness of the theoretical analysis is verified through simulations. If not otherwise specified, $\lambda = 10$, $\beta_T = 0.02$, $\tan\delta_C = 0.01$, $\tan\delta_N = 0.002$, and $g_a = 0.9$ are used in the simulations. The exact specific acoustic impedance ratio given by Eq. (31) is used in the simulations.

3.1 Validation of Optimum Values of Circuit

The simulation results using $\zeta_R = \zeta_{Ropt}$ and $\eta = 0.8\eta_{opt}$, $0.9\eta_{opt}$, η_{opt}, $1.1\eta_{opt}$, $1.2\eta_{opt}$ are shown in Figure 3(a). Only the simulation result using $\eta = \eta_{opt}$ represents $\alpha = 1$ at $g = g_a$. The simulation results using $\eta = \eta_{opt}$ and $\zeta_R = 0.01\zeta_{Ropt}$, $0.1\zeta_{Ropt}$, ζ_{Ropt}, $10\zeta_{Ropt}$, $100\zeta_{Ropt}$ are shown in Figure 3(b). Only the simulation result using $\zeta_R = \zeta_{Ropt}$ represents $\alpha = 1$ at $g = g_a$. The normal incidence sound absorption coefficient α is sensitive to the negative stiffness ratio, whereas insensitive to the resistance ratio ζ_R.

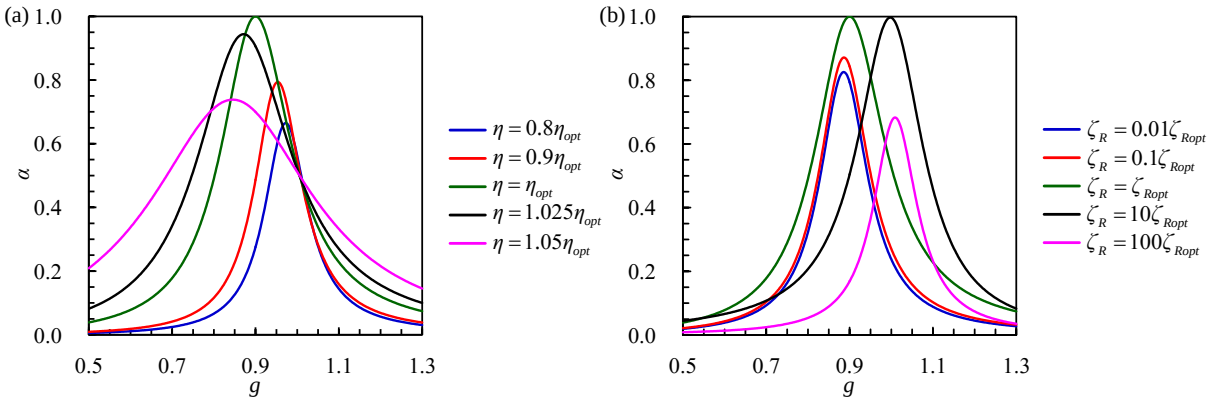

Figure 3 – Simulation results of normal incidence sound absorption coefficient with different values of negative stiffness ratio and resistance ratio.

3.2 Verification of Effect of Equivalent Stiffness Ratio and Acoustic Characteristic Impedance Ratio

The simulation results using η_{opt}, ζ_{Ropt}, and $\beta_T = 0.004$, 0.02, 0.1 are shown in Figure 4(a). The simulation results indicate that the normal incidence sound absorption coefficient α is almost independent of the equivalent stiffness ratio β_T under the optimum condition. The simulation

results using η_{opt}, ζ_{Ropt}, and $\lambda = 4$, 5, 6.7, 10, 20 are shown in Figure 4(b). The simulation results indicate that the frequency range that gives a high value of the normal incidence sound absorption coefficient is almost proportional to λ^{-1}.

The simulation results using η_{opt}, ζ_{Ropt}, and $g_a = 0.7$, 0.8, 0.9, 1 are shown in Figure 5. The simulation results indicate that the targeted frequency is tunable using the proposed method.

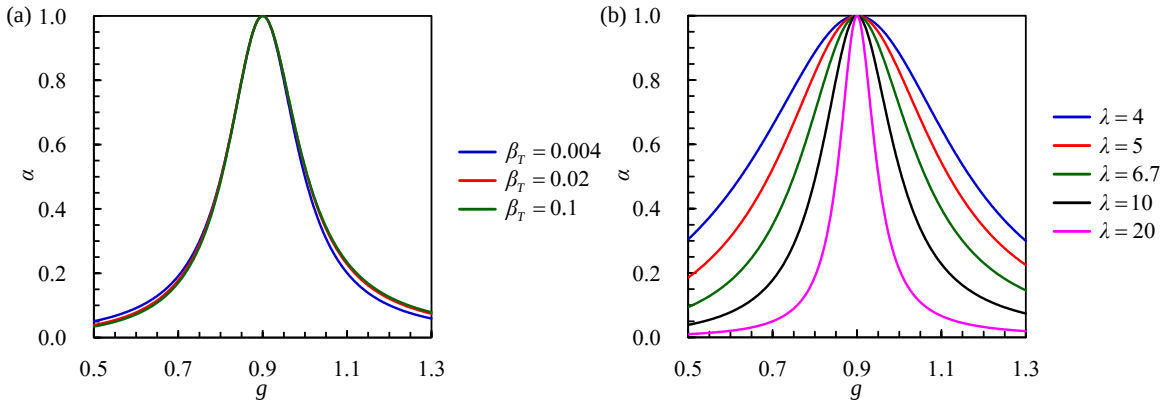

Figure 4 – Simulation results of normal incidence sound absorption coefficient with different values of equivalent stiffness ratio and acoustic characteristic impedance ratio.

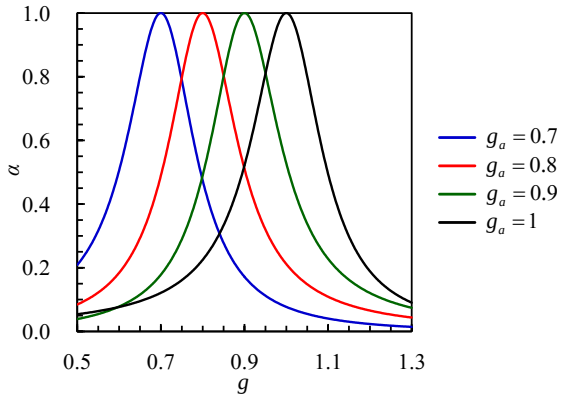

Figure 5 – Simulation results of normal incidence sound absorption coefficient with different values of targeted excitation frequency ratio.

4. EXPERIMENT

4.1 Experimental Apparatus

The schematic of the experimental apparatus is shown in Figure 6. Here l_A and l_B are the distance between the speaker and microphones A and B, respectively. The speaker on the left-hand end was used as the noise source. Four pieces of the piezoelectric elements were bonded near the center of the steel plate. All the edges of the plate were clamped. The circuit diagrams of the circuit that was coupled to the piezoelectric elements and its equivalent circuit are shown in Figure 7. The negative impedance converter was used to make the negative capacitance. The coil whose inductance is L_A and resistor whose resistance is R_B were used to stabilize the negative impedance converter in high frequency region and 0Hz, respectively. The material properties of the experimental apparatus are listed in Table 1. Here f_n is the natural frequency of the piezoelectric sound absorbing panel including the effect of the air space. Only the fixed values are listed in Table 1 with respect to the circuit. The capacitance C_N and resistance R_N in the equivalent circuit are respectively expressed as

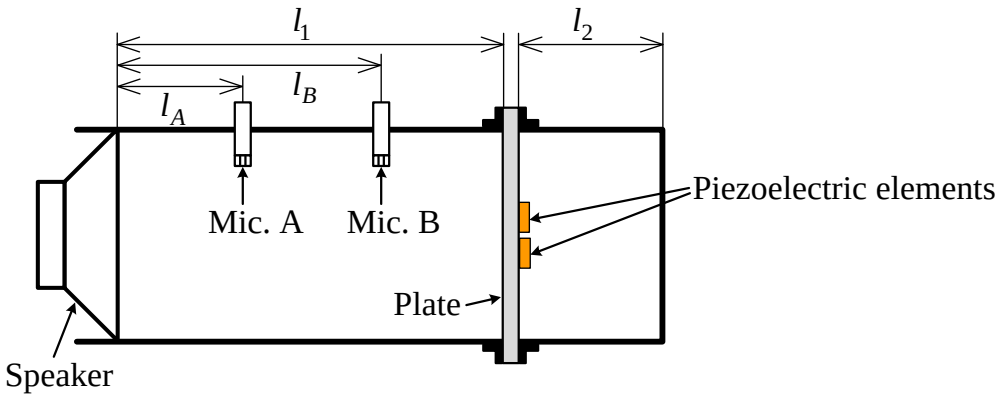

Figure 6 – Schematic of experimental apparatus.

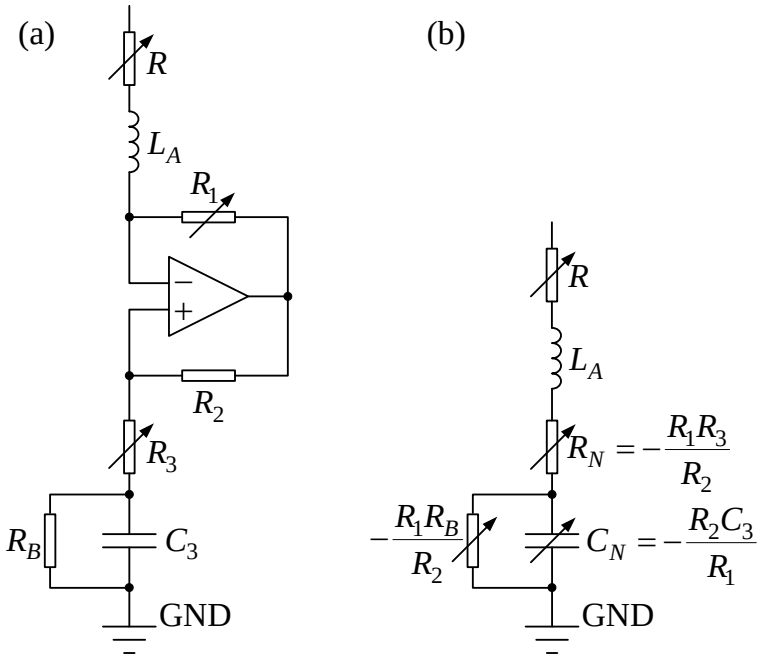

Figure 7 – Circuit diagrams used in experiment and its equivalent circuit.

$$C_N = -R_2 C_3 / R_1 \tag{43}$$

$$R_N = -R_1 R_3 / R_2 \tag{44}$$

In the experiment, the capacitance C_N was tuned by the value of R_1. After the tuning of C_N, the resistance R_N was tuned by the value of R_3. In case where the optimum resistance was positive, the variable resistor whose resistance is R was used instead of the negative resistance R_N. The equivalent mass M_b, equivalent damping coefficient D_b, and equivalent stiffness K_T were identified using the specific acoustic impedance ratio of the plate that was measured under the condition that the electrodes of the piezoelectric elements were short-circuited. The equivalent stiffness K_a was calculated using Eq. (21). The acoustic characteristic impedance ratio λ was derived using Eq. (32) and material properties of the experimental apparatus. The equivalent stiffness ratio β_T was experimentally identified (4). The equivalent electromechanical coupling coefficient was obtained using

$$\Theta_b = \sqrt{\beta_T K_T C_p} \tag{45}$$

The specific acoustic impedance ratio of the piezoelectric sound absorbing panel was expressed as

$$\bar{z} = -\mathrm{j}\left[H(\mathrm{j}\omega)\sin k(l_1 - l_A) - \sin k(l_1 - l_B)\right] / \left[H(\mathrm{j}\omega)\cos k(l_1 - l_A) - \cos k(l_1 - l_B)\right] \tag{46}$$

Table 1 – Material properties of experimental apparatus.

Acoustic tube	l_1	0.95	m
	l_2	0.084	m
	l_A	0.30	m
	l_B	0.70	m
	A	$0.30 \times 0.20 = 0.060$	m^2
	ρ_a	1.2	$\mathrm{kg/m}^3$
	c_a	343	m/s
Plate	M_b	0.65	kg
	D_b	9.0	Ns/m
	K_T	260000	N/m
	K_a	100000	N/m
	K_b	160000	N/m
	f_n	101	Hz
	γ	0.011	
	λ	17	
Piezoelectric elements (Four pieces in parallel)	β_T	0.017	
	C_p	111	nF
	$\tan\delta_C$	0.01	
	Θ_b	0.022	N/V
Circuit	L_A	2.0	H
	R_B	10	MΩ
	R_2	9.8	kΩ
	C_3	100	nF
	$\tan\delta_N$	0.002	

$$H(\mathrm{j}\omega) = P_B / P_A \tag{47}$$

where P_A is the amplitude of the sound pressure of the microphone A and P_B is the complex amplitude of the sound pressure of the microphone B (5). The normal incidence sound absorption coefficient of the piezoelectric sound absorbing panel can be derived using Eqs. (33) and (46).

4.2 Experimental Results

The experimental results of the normal incidence sound absorption coefficient are shown in Figure 8(a). The values of the circuit used in these experiments are listed in Table 2. Here f_a is the targeted frequency. The experimental result when the electrodes of the piezoelectric elements were short-circuited is also shown in Figure 8(a). The experimental results of the normal incidence sound absorption coefficient using different values of the equivalent stiffness ratio β_T are shown in Figure 8(b). In these experiments, the number of the piezoelectric elements was varied from 1 to 4. The piezoelectric elements that were not used were short-circuited. The values of the circuit used in these experiments are listed in Table 3. The experimental results show the same tendency with the simulation results.

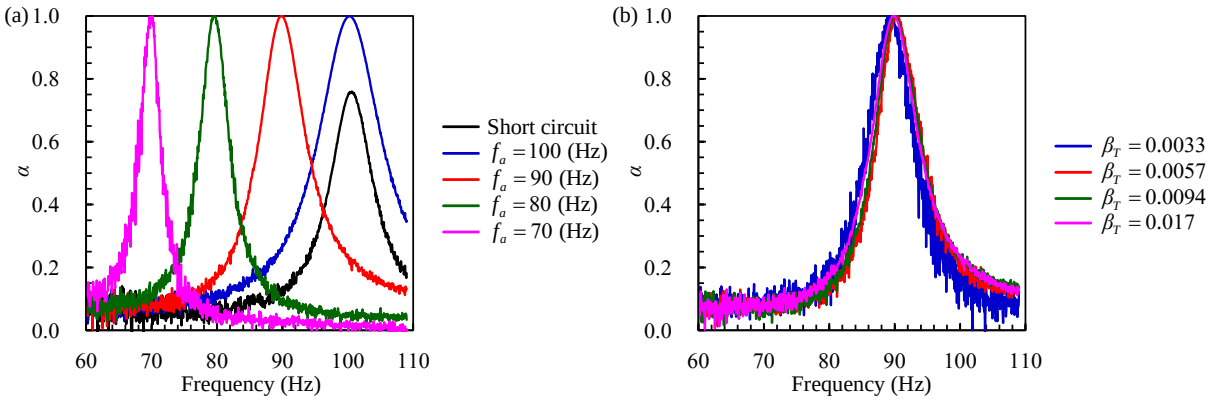

Figure 8 – Experimental results of normal incidence sound absorption coefficient with different values of targeted frequency and equivalent stiffness ratio.

Table 2 – Circuit values of experiment with different values of targeted frequency.

f_a, Hz	C_N, nF	R or R_N, Ω
70	–121	–1360
80	–124	–1320
90	–132	–1130
100	–137	–4690

Table 3 – Circuit values of experiment with different values of equivalent stiffness ratio.

Number of piezoelectric elements	β_T	C_p, nF	C_N, nF	R_N, Ω
1	0.0033	28.0	–29.6	–1500
2	0.0057	55.7	–60.5	–1810
3	0.0094	83.3	–94.6	–1700
4	0.017	111	–132	–1130

5. CONCLUSION

The method to reduce the natural frequency of the piezoelectric sound absorbing panel using the piezoelectric elements and negative capacitor was proposed. The optimum values of the negative capacitance and resistance of the circuit that is coupled to the piezoelectric elements were theoretically derived. It was found that the sound absorption performance of the proposed piezoelectric sound absorbing panel with the negative stiffness is independent of the equivalent stiffness ratio of the piezoelectric elements, and the frequency width where the high sound absorption coefficient is obtained is almost inversely proportional to the acoustic characteristic impedance of the plate. The effectiveness of the proposed method and theoretical analysis were verified through simulations and experiments.

ACKNOWLEDGEMENTS

This study was partly supported by a Grant-in-Aid for Young Scientists (B) (JSPS, No. 21760169).

REFERENCES

1. Nakazawa T., Yamada K., Matsuhisa H., Sawada K., Utsuno H. LOW-FREQUENCY NOISE REDUCTON USING A PIEZOELECTRIC SOUND ABSORBING PANEL USING LR CIRCUIT AND APPLIED VOLTAGE. Proceedings of the 11th International Conference on MOTION AND VIBRATION CONTROL, 17-19 October 2012; Fort Lauderdale, USA 2012. CD-ROM DSCC2012-MOVIC2012-8626.
2. Yamada K., Matsuhisa H., Utsuno H., Sawada K. Optimum tuning of series and parallel LR circuit for passive vibration suppression using piezoelectric elements. Journal of Sound and Vibration 2010; 329(24): 5036-5057.
3. Date M., Kutani M., Sakai S. Electrically controlled elasticity utilizing piezoelectric coupling. Journal of Applied Physics 2000; 87(2): 863-868.
4. Yamada K., Matsuhisa H., Utsuno H. A new method for accurately determining the modal equivalent stiffness ratio of bonded piezoelectric structures. Journal of Sound and Vibration 2012; 331(14): 3317-3344.
5. Chung J. Y., Blaser D. A. Transfer function method of measuring in-duct acoustic properties. Journal of the Acoustical Society of America 1980; 68: 907-921.